https://doi.org/10.5194/bg-2023-37
Preprint. Discussion started: 20 February 2023
© Author(s) 2023. CC BY 4.0 License.

Biogeosciences Discussions

Technical note: Skirt-chamber – An open dynamic method for the rapid and minimally-intrusive measurement of greenhouse gas emissions from peatlands

Frederic Thalasso[1,2], Brenda Riquelme[2,3], Andrés Gómez[2], Roy Mackenzie[2,3], Francisco Javier Aguirre[2], Jorge Hoyos-Santillan[2,4,5], Ricardo Rozzi[2], Armando Sepulveda-Jauregui[2,4,5]

[1]Departamento de Biotecnología y Bioingeniería, Centro de Investigación y de Estudios Avanzados del Instituto Politécnico Nacional (Cinvestav), Mexico City, 07360, Mexico
[2]Cape Horn International Center, Universidad de Magallanes, Puerto Williams, 6350000, Chile
[3]Millennium Institute Biodiversity of Antarctic and Subantarctic Ecosystems (BASE), Santiago, 7800003, Chile
[4]Environmental Biogeochemistry Laboratory, Centro de Investigación Gaia Antártica (CIGA), Universidad de Magallanes, Punta Arenas, 6210427, Chile
[5]Center for Climate and Resilience Research (CR)2, Universidad de Chile, Santiago, 7800003, Chile

Correspondence to: F. Thalasso (thalasso@cinvestav.mx); A. Sepulveda-Jauregui (armando.sepulveda@umag.cl)

Abstract. We present a reliable and robust open dynamic chamber for measuring greenhouse gas exchange in peatlands with minimal disturbance of the ground. This chamber, called "skirt-chamber", is based on a transparent plastic film, placed above an open frame made of sparse interwoven wires, and expanded around the base of the chamber below a steel chain that ensures contact to the ground, avoiding damage, trenching or cutting vegetation. Gas exchange is determined using a portable gas analyzer from a mass balance in which the imperfect sealing of the chamber to the ground is quantified through the injection a methane pulse. The method was tested on a pristine peatland dominated by Sphagnum magellanicum located on Navarino Island at the subantarctic Magellanic ecoregion in Chile. Our results indicate that, the skirt-chamber allowed determining methane fluxes and ecosystem respiration, in about 20 minutes, with a limit of detection of 0.185 mg CH_4 m^{-2} h^{-1}, and 173 mg CO_2 m^{-2} h^{-1}, respectively. We conclude that the skirt-chamber is a minimally-intrusive, fast, portable, and inexpensive method that allows the quantification of greenhouse gas emissions with high spatial resolution in remote locations and without delay.

1 Introduction

Peatlands are a major component of the global carbon cycle and are the largest carbon reservoir in the biosphere (Yu et al., 2011). These ecosystems hold ≈ 644 gigatons of carbon (GtC) in 399 million ha (Leifeld and Menichetti, 2018). For that reason, peatlands have gained relevance as potential Nature-based Solution (NbS) to help addressing global warming (Griscom et al., 2017; UNEP, 2019). At present, peatlands act globally as carbon sinks, sequestering 0.1 GtC y^{-1} (Frolking et al., 2011). However, peatlands are also among the largest greenhouse gas emitters to the atmosphere (IPCC, 2021) Peatlands can behave as carbon sink or net sources through time at different time scales (e.g., diurnal, seasonal, decadal, millennial)

https://doi.org/10.5194/bg-2023-37
Preprint. Discussion started: 20 February 2023
© Author(s) 2023. CC BY 4.0 License.


and spatial scales (i.e., site, watershed, region) (Ding et al., 2004; Günther et al., 2014; Cobb et al., 2017; Swails et al., 2021). The shift from sink to net source, or vice versa, depends on different factors (e.g., climatic conditions, hydrology, anthropogenic impacts) (Leifeld and Menichetti, 2018; Günther et a., 2020; Page et al., 2022). Thus, under the current context of global climate change and accelerated land use change, it is important to accurately assess whether peatlands behave as carbon sinks or net sources and for that reason it is necessary to improve the temporal and spatial resolution when measuring greenhouse gas emissions in these ecosystems (Lawson et al., 2014).

In peatlands, greenhouse gas exchanges with the atmosphere are currently determined using above-ground and ground-based methods. Above-ground methods are mostly based on the eddy covariance (EC) techniques (Aubinet et al., 2012). Ground based methods consist of chambers placed on the surface of the terrain, which allow to quantify greenhouse gas fluxes at specific locations of the ecosystem. Ground based methods involve either a discrete sampling and measurement of the chamber's headspace, or a continuous monitoring of the chamber's headspace with a gas analyzer. The use of automatic chambers, that open and close at predetermined intervals, has allowed increasing the temporal resolution (Pavelka et al., 2018). However, chamber methods also present several drawbacks; for example, the increase or decrease of the gas concentration within the chamber headspace has a direct impact on the concentration gradient between the ground and the chamber headspace, ultimately altering the flux (Kutzbach et al., 2007; Juszczak, 2013; Pirk et al., 2015; Limpert et al., 2020). Another potential drawback is that the chambers sometimes do not include a fan to homogenize the air, causing local gradients, which modify the measured fluxes, underestimating them by at least one-third (Christiansen et al., 2011; Juszczak, 2013; Pavelka et al., 2018). More importantly, chambers require to be well sealed to avoid gas exchange between the atmosphere and the chamber headspace. To avoid leakiness, chambers are usually installed on a collar that drives several centimeters into the ground, sometimes combined with a water-filled groove.

The use of collars presents additional drawbacks, especially in peatlands characterized by uneven terrain and a dense vegetation rug. First, the collar installation implies some disturbance of the ecosystem, such as cutting the vegetation around the collar to allow its penetration into the ground. This procedure creates a trenching effect that must be considered in measurement protocols (Järveoja et al., 2020). Thus, after collar installation, it is a common practice to wait between 24 to 48 h before starting flux measurements. A collateral impact of the collar strategy is that, due to the delay in measurement, it significantly limits the number of locations where flux can be measured in each experimental timeframe, thus limiting both the temporal and spatial resolution of the studies, particularly in remote areas. Second, chamber installation would generally be preferred in relatively flat and even terrain over sloped or uneven ground, thus involving a bias selection of the locations where fluxes are measured. Third, automatic chambers are relatively expensive, thus most of the studies involving them use a few simultaneous chambers operated over days to weeks. This strategy offers an excellent temporal resolution but a relatively poor spatial resolution that could potentially lead to pseudoreplication, i.e. replicates not statistically independent.

To elude the former drawbacks, half a century ago, Edwards and Sollins (1973) suggested a new concept of chamber through which a known carrier gas flows continuously. The gas concentration is measured at the outlet of the chamber and the flux is determined after resolving a mass balance equation that involves all inputs and outputs of the chamber. According to the

https://doi.org/10.5194/bg-2023-37
Preprint. Discussion started: 20 February 2023
© Author(s) 2023. CC BY 4.0 License.


Livingston and Hutchinson's classification (Livingston and Hutchinson, 1995), that concept corresponds to a steady-state through-flow chamber, called "open dynamic chamber" (ODC), by opposition to standard static and dynamic chambers, which are non-steady-state chambers. The advantages of ODCs include a limited gas concentration buildup in the chamber and the continuous measurement of flux over the deployment time. More importantly, ODC measurements are not affected by leaks, as far as the carrier gas composition and flow is precisely known (see Section 2.1 for details). Thus, ODCs have the potential to elude the strict requirement of hermetic sealing and, therefore, to avoid disturbances and measurement delay caused by collar installation. Furthermore, the carrier gas of standard ODCs could be substituted by the natural air exchange caused by imperfect sealing of the chamber exposed to wind, as far as the flowrate of the air exchange is known. The substitution of a carrier gas for the quantification of the gas exchange with the environment would allow to avoid the use of heavy gas cylinders, advantageous for the rapid deployment of a simple, low-cost chamber able to quantify greenhouse gas emissions or capture, by simply positioning the chamber on the surface of the peatland without penetration into the ground. This chamber could be then placed on any surface, independently of the vegetation cover, slope or terrain unevenness.

The objective of this study was to present the test concept of a modified ODC, called hereinafter the "skirt-chamber", referring to the plastic skirt that is used to make contact with the ground. We tested the skirt-chamber design in the laboratory and in a peatland dominated by *Sphagnum magellanicum* on Navarino Island (Lat. 55°S), in the sub-Antarctic Magellanic ecoregion of Chile, characterized by an oceanic climate (Rozzi et al., 2012). Our research focused on evaluating the capacity of the skirt-chamber to measure CH_4 and CO_2 net emissions/capture, as well as the respiration rates of the ecosystem at different vegetation covers and terrain. In addition, one of our main goals was to develop a reliable and robust tool that was easy to operate and transport to remote areas, where data about the gas exchanges between peatlands and the atmosphere are limited.

2 Materials and methods

2.1. Skirt-chamber

The skirt-chamber (Fig. 1, details provided in Section 2.3) consists of an open frame made of sparse interwoven steel wires, whose purposes are supporting a transparent plastic film and defining the chamber´s volume while allowing light penetration. On top of the frame (installed on the ground, facing down), the plastic film is expanded over the frame and fixed at its base. When installing the chamber on the ground, the plastic film is expanded on the ground around the chamber and a steel chain is placed above it, surrounding three times the base of the chamber, to ensure that the plastic film is in contact with the ground. Thus, this design creates a fixed volume chamber, opened at the bottom and in contact with the ground. Inside the chamber, a fan is placed to homogenize the air content. Inlet and outlet ports are fixed on opposite sides of the frame and connected, in a recirculation mode, to a laser ultraportable greenhouse analyzer (*i.e.* UGGA, model 915-0011-1000, Los Gatos Inc., San Jose, CA, USA).

The gas mass balance of the skirt-chamber can be described by Equations 1−3;

https://doi.org/10.5194/bg-2023-37
Preprint. Discussion started: 20 February 2023
© Author(s) 2023. CC BY 4.0 License.

Biogeosciences Discussions Open Access EGU

$$\frac{dC_C}{dt} = inlets - outlets = flux + leak\ inlet - leak\ outlet \quad (1)$$

$$\frac{dC_C}{dt} = F \cdot \frac{A_C}{V_C} + \frac{Q_L}{V_C} \cdot C_L - \frac{Q_L}{V_C} \cdot C_C \quad (2)$$

$$\frac{dC_C}{dt} = F \cdot \frac{A_C}{V_C} + \frac{Q_L}{V_C} \cdot (C_L - C_C) \quad (3)$$

Where C_C is the gas concentration inside the chamber (mg m^{-3}); F is the flux between the chamber and the ground (mg m^{-2} h^{-1}); A_C is the area of the chamber in contact with the ground (m^2); V_C is the chamber volume (m^3); Q_L is the flowrate of the gas exchange between the chamber and the exterior, caused by the imperfect seal between the chamber and the ground, (m^3 h^{-1}); and, C_L is the gas concentration outside de chamber at ground level.

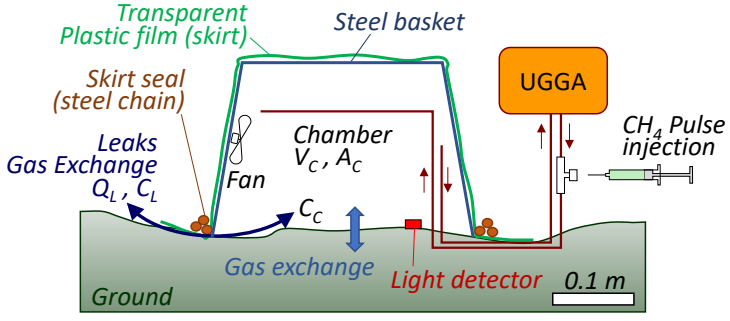

Figure 1. Skirt-chamber concept (see text for details).

The term Q_L/V_C is the dilution rate caused by the gas exchange between the chamber and the environment (Eqs. 2, 3), which is the inverse of the mean gas residence time in the chamber (θ_C), in such manner that Equation 3 becomes;

$$\frac{dC_C}{dt} = F \cdot \frac{A_C}{V_C} + \frac{(C_L - C_C)}{\theta_C} \quad (4)$$

At equilibrium, *i.e.* concentration not changing over time, dC_C/dt equals zero, the concentration of the gas in the chamber can be considered as the constant C_B (baseline concentration). Under these conditions, Equation 4 becomes;

$$F = -\frac{(C_L - C_B)}{\theta_C} \cdot \frac{V_C}{A_C} = \frac{(C_B - C_L)}{\theta_C} \cdot \frac{V_C}{A_C} \quad (5)$$

Thus, as V_C and A_C are known, F can be determined during chamber deployment from the measurement of C_L, C_B, and θ_C. θ_C can be determined in the field through the injection of a gas pulse within the chamber. Under these conditions, the steady-state is lost and by substitution of F (Eq. 5) in Equation 4, we obtain Equation 6;

$$\frac{dC_C}{dt} = -\frac{(C_L - C_B)}{\theta_C} \cdot \frac{V_C}{A_C} \cdot \frac{A_C}{V_C} + \frac{(C_L - C_C)}{\theta_C} = \frac{(C_B - C_C)}{\theta_C} \quad (6)$$

Since C_B is a constant, under fixed experimental conditions, Equation 6 can be rewritten as follows;

$$\frac{d(C_B - C_C)}{(C_B - C_C)} = -\frac{dt}{\theta_C} \quad (7)$$

And, after integration over time t, we obtain;

$$C_{c,t} = C_B + (C_{C,0} - C_B) \cdot e^{\left(-\frac{t}{\theta_C}\right)} \quad (8)$$

https://doi.org/10.5194/bg-2023-37
Preprint. Discussion started: 20 February 2023
© Author(s) 2023. CC BY 4.0 License.


Where $C_{C,t}$ and $C_{C,0}$ are the gas concentration within the chamber, at time t and shortly after the injection of a gas pulse, respectively. Equation 8 describes how, after a gas pulse has been injected, C_C return asymptotically to the equilibrium concentration C_B. Thus, the injection of a gas pulse allows to determine θ_C, which can be then used to estimate F by using Equation 5. The step-by-step field methodology is described in section 2.3.

2.2. Study site and campaign

The selected study site (54.9396°S; 67.6419°W) is a 46,000 m^2 peatland, locally called "Omora peatland" in reference to the Omora Ethnobotanical Park (Rozzi et al., 2006) where it is located, at 2 km west of Puerto Williams, on the northern coast of Navarino Island. This peatland has been also previously called "Caleta Bacalao" in a detailed study of the late quaternary vegetation and climate (Heusser et al., 1989). In that study, the age of the peatland has been established to a maximum of 13,000 y B.P. This ombrotrophic elevated peatland is dominated by *Sphagnum magellanicum*, with a hummocky topography covered by irregular patches of *Empetrum rubrum*, *Gaultheria* spp., *Marsippospermum grandiflorum*, *Tetroncium magellanicum*, *Polytrichum* spp. and shrubby Antarctic beech (*Nothofagus antarctica*). Also, several lichen species common to the Magellanic moorland complex were extensively covering the peatland, such as *Pseudocyphelaria* spp., *Cladonia* spp. and *Ochrolechia* spp. In some locations, apparent black peat was observed without a living *Sphagnum* cover. The depth of the peat layer was measured from 3 to 10 m, and the section where measurements were made was characterized by a depth of 8 ± 1 m. The peatland was not flooded but the water table was close to the surface, *i.e.* 0.1−0.6 m. The campaign took place on March 3−24, 2022, which corresponds to the end of summer season. To minimize the impact of operators on the peatland superficial structure, operators were using snowshoes and each measurement spot was marked prior to measurements, to avoid stepping over the terrain.

2.3. Chamber design and fluxes measurements

The chamber was a pyramidal trunk basket with a base (opening) of 0.32 × 0.29 m, and a height of 0.22 m (Model 47970, Spectrum, Mexico). Above the chamber, we positioned a low-density polyethylene film (1.4 × 1.4 m; 0.025 mm thick; Frost King, Mexico). The plastic film was adjusted and fixed to the chamber´s bottom (Fig. S1). The chamber was equipped with a battery-operated fan (Portable Fan, Cazokasi, Mexico), which was fixed on a lateral face of the chamber (opposite side from the sun) and operated at an airflow speed of 1.2 m s^{-1}. Inside the chamber, a light/temperature data logger was installed at ground level (MX2202, Hobo, USA), and a second one was installed on the top of the chamber. Data loggers recorded visible light intensity in Lux units. Inside the chamber, two 6 mm external diameter (4 mm internal diameter) flexible polyurethane tubing (PUN-6X1-DUO-BS, Festo, Mexico) were fixed on opposite faces of the basket, at about two-thirds of the chamber´s height, passed from below the edge of the chamber and connected the UGGA. The UGGA measured CH_4 and CO_2 concentration at a 1 Hz frequency. When fluxes were measured, the chamber was placed face down, the plastic skirt was expanded around the chamber and a steel chain (0.27 kg m^{-1}) was placed above the plastic film, surrounding three times

https://doi.org/10.5194/bg-2023-37
Preprint. Discussion started: 20 February 2023
© Author(s) 2023. CC BY 4.0 License.

the base of the chamber to ensure that the plastic film was in contact with the ground. At the end of each experiment, a dark screen was placed above the chamber, to measured CO_2 flux in absence of light (respiration from soil and plants).

Flux measurements involved a four steps protocol (Table 1).

Step 1, the ground air concentration (C_L) of CH_4 ($C_{L,CH4}$) and CO_2 ($C_{L,CO2}$) was measured for 5 min, just above the vegetation cover (where the chamber was placed).

Step 2, the chamber was positioned on the ground and, once steady state was reached, C_B of CH_4 ($C_{B,CH4}$) and CO_2 ($C_{B,CO2}$) were measured over a 5 minutes period. It should be noted that, after pulse injection (third step), a second $C_{B,CH4}$ was determined. Thus $C_{B,CH4}$ determined during this step 2, was renamed $C_{B,CH4,1}$.

Step 3, a pulse of 1 mL of standard CH_4 (99.99%, Linde, Chile) was injected with a plastic syringe through a septum connected on the waste line of the UGGA (returning to the chamber). The decreasing section of CH_4 concentration was used to calibrate Equation 8, and to determine θ_C and $C_{B,CH4}$, the latter being in this case $C_{B,CH4,2}$. This step was maintained for 5 to 7 minutes, until a stable $C_{B,CH4,2}$ was observed. It should be also noted that, as we will show in the results section, the pulse injection (*i.e.*, step 3) had no effect on the CO_2 concentration within the chamber. Thus, $C_{B,CO2}$ could be determined over the entire period of steps 2 and 3.

Step 4, a dark screen was placed on the chamber for 5 minutes to measured CO_2 flux in absence of light (respiration). This new CO_2 steady state concentration was called $C_{D,CO2}$; where D stands for dark conditions. As we will show in the results section, the dark screen had no apparent effect on the CH_4 concentration within the chamber. Therefore, $C_{B,CH2,2}$ could be determined throughout steps 3 and 4 (Table 1).

The four steps experimental strategy allowed to determine three key CH_4 concentrations ($C_{L,CH4}$, $C_{B,CH4.1}$, and $C_{B,CH4.1}$) that were used to determine two equivalent CH_4 fluxes ($F_{CH4,1}$ and $F_{CH4,2}$; Eq. 5, Table 1). Similarly, three key CO_2 concentrations ($C_{L,CO2}$, $C_{B,CO2}$, and $C_{D,CO2}$) were determined, providing one CO_2 flux and one respiration rate (F_{CO2} and R_{CO2}, respectively) using Equation 5 in both cases.

Table 1: Experimental strategy, parameters and fluxes determined (see text for details).

		Step 1	Step 2	Step 3	Step 4
CH_4	Parameters	$C_{L,CH4}$	$C_{B,CH4,1}$	$C_{B,CH4,2}$	
	Fluxes	$F_{CH4,1}$		$F_{CH4,2}$	
CO_2	Parameters	$C_{L,CO2}$	$C_{B,CO2}$		$C_{D,CO2}$
	Fluxes	F_{CO2}			R_{CO2}

https://doi.org/10.5194/bg-2023-37
Preprint. Discussion started: 20 February 2023
© Author(s) 2023. CC BY 4.0 License.


2.4. Calibration and laboratory experiments

The chamber volume was experimentally checked in the laboratory (no wind) and on a flat surface, which minimizes leakage. Pulses of known volumes of CH_4 were injected and the concentration into the chamber was measured. The concentration curve was well modeled using the Levenspiel's equation (Levenspiel, 1999) for two continuous stirred tank reactors in series (Eq. 9).

$$C_t = C_p \cdot \left(\frac{t}{\theta}\right) \cdot e^{\left(\frac{-t}{\theta}\right)} = \frac{M_p}{V_C} \cdot \left(\frac{t}{\theta}\right) \cdot e^{\left(\frac{-t}{\theta}\right)} \quad (9)$$

Where C_t is the concentration at time t, and C_p is the initial pulse concentration within the chamber, which is equal to the mass of CH_4 injected during the pulse (M_p) divided by V_C. In Equation 9, C_p and θ were the adjustment parameters calibrated numerically (Section 2.5).

In each experiment, both in the laboratory and field, the area covered by the skirt-chamber was determined from a scaled photograph of the chamber taken from above and assuming that the perimeter of the chain used to maintain the skirt in contact to the ground defined the area. The scaled photographs were treated using ImageJ (v. 1.8.0_172).

The skirt-chamber method was validated in the field, *i.e.* on uneven terrain and exposed to wind. With that purpose, quadruplicate pulses of six known CH_4 mass (M_p) were injected into the chamber. The mass of CH_4 detected, in excess to the baseline, was determined through integration (Eq. 10) and compared to the mass injected. An equivalency between the mass of CH_4 injected and the mass of it that is detected would indicate that the mass balance of the chamber is correct and that any amount of gas reaching the chamber is correctly appraised.

$$M_p = \int_0^t \left(C_{c,t} - C_B\right) \cdot \left(\frac{V_C}{\theta_C}\right) \cdot dt \quad (10)$$

2.5. Data treatment and statistical analysis

Equations 8, 9, and 10 were calibrated to experimental data using a Generalized Reduced Gradient (GRG) Nonlinear tool and minimizing the root mean square error (RMSE) between experimental data and models. To estimate uncertainties of flux determinations (based on Eq. 5), we considered the uncertainties linked to the measurements of the gas concentration at ground level (σC_L) and of the baseline concentration (σC_B) using a propagation of error approach (Eq. 11), where σ_F is the standard deviation of the flux determination.

$$\sigma_F = \frac{\sigma_{(C_L - C_B)}}{\theta_C} \cdot \frac{V_C}{A_C} = \frac{\sqrt{{\sigma_{C_L}}^2 + {\sigma_{C_B}}^2}}{\theta_C} \cdot \frac{V_C}{A_C} \quad (11)$$

In order to estimate the temporal and spatial variability of flux measurements on different days and locations, we used the mean coefficient of variation (CV), which is defined as the ratio of the standard deviation to the mean. When comparing fluxes measured with different methods and their corresponding CV, data were Log_{10} transformed to fulfil the normality condition assessed by Saphiro Wilk test. Then, we determined significant differences among variables using independent samples t-Test to with a $p < 0.05$. Model calibrations and statistical analyses were performed with Origin(Pro) OriginLab

https://doi.org/10.5194/bg-2023-37
Preprint. Discussion started: 20 February 2023
© Author(s) 2023. CC BY 4.0 License.


Corporation (Version 2016, Northhampton, USA). Regarding the limit of detection (LOD) of the skirt-chamber method, we used the typical arbitrary limit of a minimal signal at least three times above standard deviation, thus corresponding to a CV below 33%. Measurements obtained with a higher CV were considered uncertain.

3. Results and discussion

3.1. Performance of the skirt-chamber

An example of chamber deployment in the field and the corresponding data obtained at a location where high emission was observed is shown on Figure 2. During step 1, before chamber deployment, the CH_4 and CO_2 concentrations at ground level, *i.e.* $C_{L,CH4}$ and $C_{L,CO2}$, respectively, were registered. Immediately after chamber deployment (step 2), an increase of CH_4 concentration was standardly observed, at a new level $C_{B,CH4,1}$, which is an indicator of CH_4 emissions. On the contrary, the CO_2 concentration decreased to a level $C_{B,CO2}$, often below $C_{L,CO2}$, which is an indication of CO_2 capture. On step 3, as expected, the injection of a CH_4 pulse caused a sudden increase of CH_4 concentration, followed by an asymptotic and slow return to the baseline level $C_{B,CH4,2}$. Then, the use of a dark screen (step 4), caused an increase of the CO_2 concentration at $C_{D,CO2}$, above $C_{L,CO2}$, which is a manifestation of respiration without photosynthetic uptake. Notably, it was observed that the CH_4 pulse injection during step 3 had no effect on the CO_2 concentration, and conversely, the dark screen installed during step 4 had no effect on CH_4 concentration, in such manner that to improve the quality of our data, $C_{B,CH4.2}$ was determined using data from steps 3 and 4, while $C_{B,CO2}$ was determined with data from steps 2 and 3 (Table 1).

https://doi.org/10.5194/bg-2023-37
Preprint. Discussion started: 20 February 2023
© Author(s) 2023. CC BY 4.0 License.

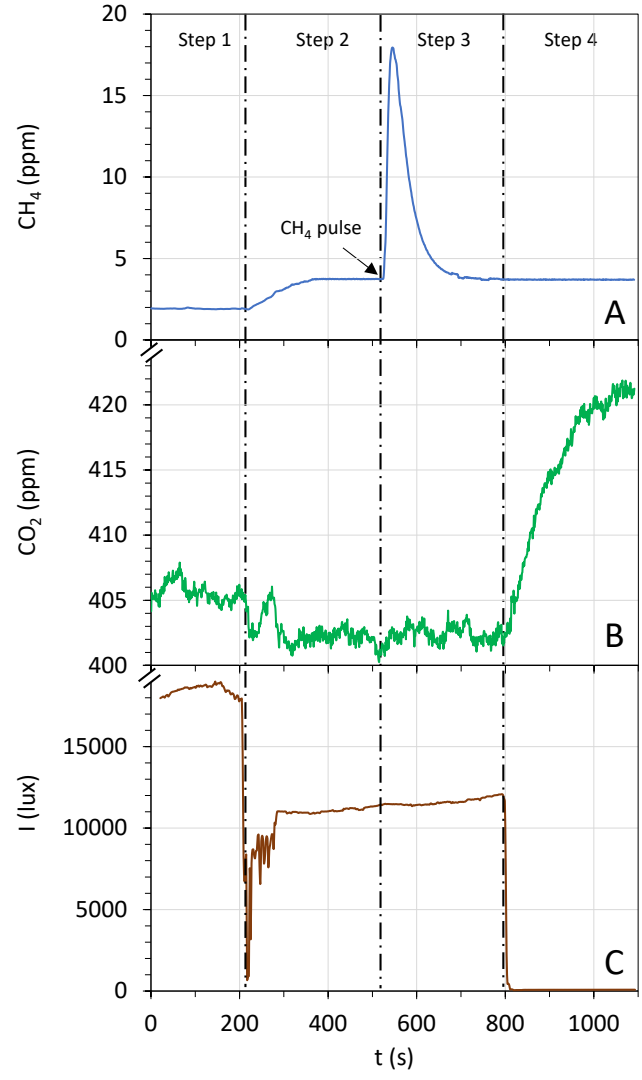

225

Figure 2. Example of data obtained during a chamber deployment; (A) CH_4 concentration, (B) CO_2 concentration, and (C) visible light irradiance. See text for a complete description of the four steps.

3.2. Calibration and method validation

In general, after pulse injections, Equation 8 fitted well the experimental data and over 130 measurements, the mean
230 coefficient of determination (R^2) value between the model and the experimental data was 0.987 ± 0.055, (mean ± σ), suggesting that the skirt-chamber acted as a continuously stirred tank reactor. Overall, θ_C was estimated at 30.74 ± 22.70 s during the entire field campaign. Reminding that $\theta_C = V_C/Q_L$, the equivalent gas flow rate exchange between the chamber and the environment (leak flowrate) was 0.67 ± 0.49 L s^{-1}. By comparison, during laboratory testing, over a flat surface and under no wind conditions, θ_C was estimated to 327.13 ± 11.24 s (n = 5), which corresponded to an exchange flowrate of

https://doi.org/10.5194/bg-2023-37
Preprint. Discussion started: 20 February 2023
© Author(s) 2023. CC BY 4.0 License.

235 0.063 ± 0.002 L s^{-1}, *i.e.* ten time lower than in the field. These results suggest that the design of the skirt-chamber, simply placed on top of the vegetation rug and under non-flooded conditions, promoted a large air exchange with the environment, probably due to wind flushing the interwoven stems, leaves, and roots, at the surface of the peatland and beneath the plastic skirt. This has been the subject of a report from Lai et al. (2012) who stressed-out the importance of wind effects and might be a potential advantage of the skirt-chamber compared to standard chambers using collars, where wind effects are impeded.

240 During field deployment, a set of validation experiments was performed through the injection of quadruplicate CH_4 samples at six distinct concentrations. In each case, $C_{B,CH4,2}$ and θ_C were estimated through Eq. 8 and then the mass of CH_4 detected in the skirt-chamber (M_p) was estimated using Eq. 10. The results obtained are presented in Figure 3, showing that R^2 was 0.997 and the slope of the mass of CH_4 detected vs. the mass injected was 0.977. The equivalency between the mass of CH_4 injected and detected indicates that the mass balance of the skirt-chamber (Eq. 3) correctly describes the behavior of the

245 skirt-chamber and that any amount of gas reaching the chamber is correctly accounted for, validating the method.

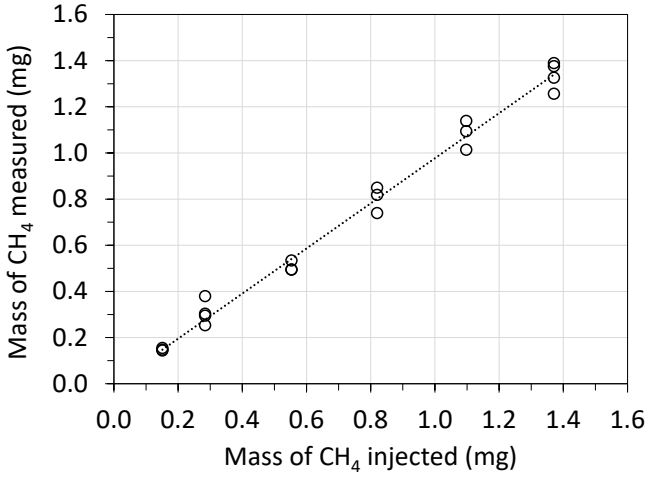

Figure 3. Validation of the skirt-chamber through the injection of CH_4 pulses at different concentrations, and determination of mass of CH_4 detected in the chamber.

3.3. CH_4 emission

250 As previously mentioned, Equation 5 used to determine CH_4 flux can be applied from $C_{L,CH4}$ and $C_{B,CH4,1}$ to determine $F_{CH4,1}$ or alternatively $C_{L,CH4}$ and $C_{B,CH4,2}$ to determine $F_{CH4,2}$. We observed that $F_{CH4,1}$ was subject to large variations, with a mean CV of 171 ± 370%, over 130 measurements. Contrastingly, $F_{CH4,2}$ was characterized by a mean CV of 30 ± 38%. We hypothesize that the large difference in CV between $F_{CH4,1}$ and $F_{CH4,2}$ was due to two factors. First, $C_{B,CH4,1}$ was determined during step 2, shortly after positioning the chamber, while $C_{B,CH4,2}$ was determined during step 3, at least 5 minutes after the

255 chamber was installed. Second, $C_{B,CH4,1}$ was determined from a shorter period of time (3 to 4 minutes) while $C_{B,CH4,2}$ was determined from a longer period, i.e. periods 3 and 4, lasting 8 to 9 minutes. From these results, only $F_{CH4,2}$ was considered hereafter.

https://doi.org/10.5194/bg-2023-37
Preprint. Discussion started: 20 February 2023
© Author(s) 2023. CC BY 4.0 License.

To evaluate the repeatability of our measurements, five measurements of $F_{CH4,2}$ were done over a short period of time (< 1.5 h) in two locations where relatively high and low emissions were observed. At the relatively high emission hotspots, $F_{CH4,2}$ was 17.10 ± 1.77 mg m^{-2} h^{-1} (CV 10.3%) while at the relatively low emission spot, $F_{CH4,2}$ was 1.20 ± 0.89 mg m^{-2} h^{-1} (CV 74.6%). Repeatability within a longer time frame was also evaluated with measurements at 16 locations divided in four transects of 3 m, thus separated by about 1 m. These measurements were repeated on three occasions, *i.e.* 2 and 12 days after the first measurement (Table 2). During these measurements, we observed that the temporal variation (same location at different days) was characterized by a mean CV of 59 ± 21% while the mean CV of spatial variation (different locations on the same day) was 220 ± 34%. In particular, it was observed that the CH_4 hotspots, *i.e.* the three locations among the 16 measured where the higher fluxes were observed, did not change over time. These results suggest that the spatial variation was higher than temporal variation and that the skirt-chamber successfully detected hotspots in repeated occasions.

Table 2: $F_{CH4,2}$ measured at 16 locations divided in four transects, on three occasions, *i.e.* at t = 0, 2, and 12 days. *: hotspots.

		t (d)			
#	Transect	0	2	12	CV
1	1	0.239 ± 0.127	0.06 ± 0.034	0.368 ± 0.049	70%
2	1	0.191 ± 0.037	0.078 ± 0.083	0.224 ± 0.065	47%
3	1	1.069 ± 0.047	0.053 ± 0.07	0.744 ± 0.058	83%
4	1	0.564 ± 0.108	0.005 ± 0.042	0.326 ± 0.031	94%
5	2	1.911 ± 0.14	0.687 ± 0.114	0.808 ± 0.117	59%
6	2	8.026 ± 0.529*	5.338 ± 0.99*	4.446 ± 0.719*	31%
7	2	0.307 ± 0.091	1.477 ± 0.077	0.676 ± 0.148	73%
8	2	3.880 ± 0.233	0.938 ± 0.133	3.15 ± 0.299	58%
9	3	30.600 ± 1.840*	44.980 ± 2.454*	19.215 ± 0.845*	41%
10	3	1.07 ± 0.093	1.907 ± 0.110	0.120 ± 0.062	87%
11	3	6.708 ± 0.283*	5.097 ± 0.817*	5.912 ± 0.370*	14%
12	3	1.753 ± 0.032	2.806 ± 0.232	1.254 ± 0.112	41%
13	4	1.284 ± 0.135	1.997 ± 0.07	0.417 ± 0.045	64%
14	4	0.134 ± 0.04	0.170 ± 0.057	0.351 ± 0.04	53%
15	4	1.570 ± 0.087	2.060 ± 0.09	0.323 ± 0.053	68%
16	4	0.485 ± 0.136	0.311 ± 0.119	0.107 ± 0.082	63%
	Mean	3.737 ± 7.533	4.248 ± 10.992	2.403 ± 4.799	28%
	CV	202%	259%	200%	

https://doi.org/10.5194/bg-2023-37
Preprint. Discussion started: 20 February 2023
© Author(s) 2023. CC BY 4.0 License.

Biogeosciences Discussions Open Access EGU

The error on $F_{CH4,2}$ determination was evaluated through CV (Eq. 11; Fig. 4A). As flux is determined from the difference of C_L and C_B, the smaller is that difference, the smaller is the flux and the larger is the impact of measurement noise. Overall, CV ranged from 1 to 207% with a mean of 30 ± 38%, with obvious larger CV for lower fluxes. It is worth noting that large errors on low flux measurements would have a relatively little impact on the mean emission that would be attributed to a peatland, particularly if it includes hotspots. For instance, in the set of 16 measurements (Table 2), the three locations with the larger emissions represented 76-82% of the total emissions. Thus, the remaining 18-24% of the emissions were distributed among 13 relatively low emission spots, for which a measurement error has a little specific weight. To illustrate the latter, based on our complete dataset (130 measurements), we determined how the variation in each measurement, propagates to the mean emission of the complete dataset ($\bar{F}_{CH4,2}$; Figure 4B). Clearly, although hotspots are characterized by a lower CV, they have a much larger impact on the mean emission, compared to low emission spots. Hotspots must therefore be the object of a closer attention, when determining the mean emission of a peatland. As it will be discussed in section 3.6, this is a potential strength of the skirt-chamber, because it allows to multiply the number of locations that can be characterized in a given timeframe, offering a higher probability to detect hotspots.

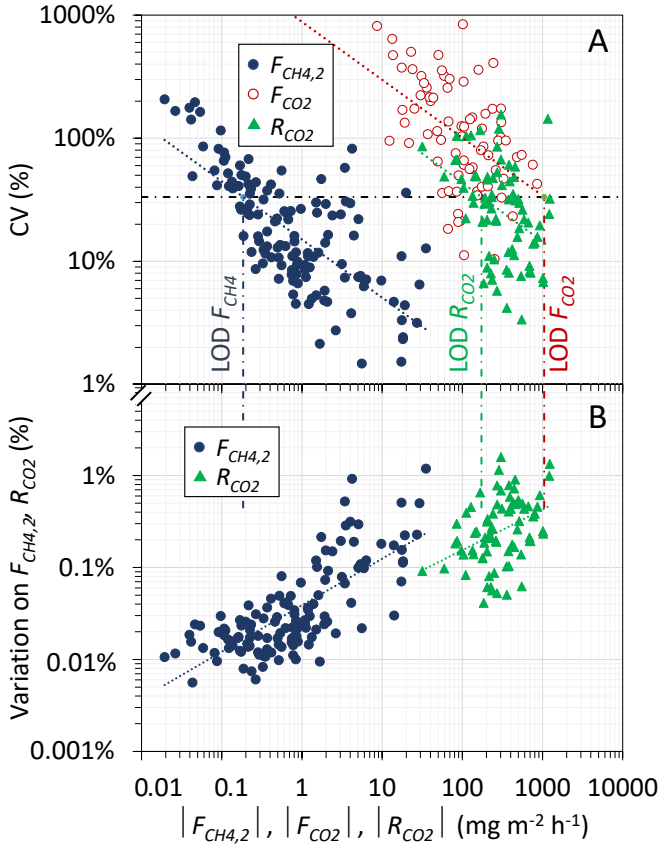

Figure 4. Impact of the absolute magnitude of flux and respiration on the coefficient of variation (CV), and limit of detection of the method (LOD; A); impact of each $F_{CH4,2}$ measurement of the mean emission of the complete dataset (B).

https://doi.org/10.5194/bg-2023-37
Preprint. Discussion started: 20 February 2023
© Author(s) 2023. CC BY 4.0 License.


Regarding the LOD of the CH_4 flux determination, we used the typical arbitrary limit of a CV below 33%. This was the case of 71 % of our complete set of $F_{CH4,2}$ measurements. When applying the CV limit to the power trendline that best fitted our experimental data ($CV = 0.15 \cdot F_{CH4,2}^{-0.472}$; Fig. 4A), we estimated that the LOD of $|F_{CH4,2}|$ was 0.185 mg m^{-2} h^{-1}, and 81% of our complete dataset (n=130) was above that LOD. If considering all measurements inferior to LOD uncertain and equal to zero, the mean emission of the whole dataset was reduced by only 0.7%. Thus, as previously established, measurements with low significance had a negligible impact on the mean emission.

Overall, the CH_4 flux ranged between -4.23 and 35.26 mg m^{-2} h^{-1}, with a mean magnitude of 2.68 ± 6.05 mg m^{-2} h^{-1}. This range is consistent with values reported in previous measurements conducted in peatlands from Southern Patagonian, which were ranging between -0.03 and 17.30 mg m^{-2} h^{-1} (Münchberger et al., 2019; Barret et al., 2022). Approximately 80% of CH_4 fluxes were below those reported by Münchberger et al. (2019) Lehmann et al. (2016) and Fritz et al. (2011) using the static chamber method. Our CH_4 fluxes are also in the same order of magnitude of fluxes reported from bogs and fens in northern regions (0.03 to 23.43 mg m^{-2} h^{-1}) (Abdalla et al., 2016). However, the highest fluxes we measured are comparable in magnitude to the largest reported in tropical peatlands (Ribeiro et al., 2021); for example, in Panama (31 and 48 mg m^{-2} h^{-1}) (Wright et al., 2013; Hoyos-Santillan et al., 2019) and in Venezuela (40.03 mg m^{-2} h^{-1}) (Bracho et al., 1990). Negative values were observed in 11% of measurements, most of them being close to the detection limit of the method. When excluding negative values, the range of CH_4 emissions covered three orders of magnitude, sometimes on very close locations.

3.5. CO_2 emissions

Overall, CO_2 readings were subject to a higher noise level, compared to CH_4 readings, and therefore F_{CO2} presented higher variability. Overall, F_{CO2} was negative in 54% of the cases, and ranged between −857 and 549 mg m^{-2} h^{-1}, with a mean of −21.56 ± 208.49 mg m^{-2} h^{-1}. This large variability was reflected in the CV of the absolute F_{CO2}, noted $|F_{CO2}|$ (Fig. 4A), which were significantly higher that the corresponding CV of $F_{CH4,2}$ ($p < 0.05$). In this case, the LOD of $|F_{CO2}|$ was estimated to 1,047 mg m^{-2} h^{-1} and none of our measurements was above that limit. Moreover, only 10% of our measurements presented a CV inferior to 33.3%. These results are strong evidence that the skirt-chamber, in it present configuration, failed in estimating accurately the CO_2 exchange between the peatland and the atmosphere. Several reasons could be put forward. First, as it will be shown in section 3.5, on the contrary to $C_{B,CH4}$, $C_{B,CO2}$ was highly dynamic and dependent on the solar irradiance, which was rapidly changing over time during the field campaign. Second, the skirt-chamber tested used a transparent plastic film over a basket made of sparse interwoven steel wires, which limited the amount of light reaching the ground to 54 ± 8%. Thus, photosynthesis was considerably limited, and clearer results might have been obtained with a more transparent chamber design, and under more stable weather conditions.

https://doi.org/10.5194/bg-2023-37
Preprint. Discussion started: 20 February 2023
© Author(s) 2023. CC BY 4.0 License.


3.5. Ecosystem respiration

As illustrated on Figure 2, when covering the skirt-chamber with a dark screen, an increase of the CO_2 concentration within the skirt-chamber was standardly observed, reaching a new steady state at $C_{D,CO2}$. This behavior was observed in all cases and suggested that the respiration rate can be measured during field deployment of the skirt-chamber. The dark screen limited light penetration by 98.4 ± 1.8%, in such manner that photosynthesis could be considered insignificant. The change of the CO_2 concentration, from $C_{B,CO2}$ to $C_{D,CO2}$, was relatively fast and followed an asymptotic trend similar to Eq. 8 (Eq. 12), where $C_{C,CO2,t}$ is the CO_2 chamber concentration at time t, and θ_D is the response time.

$$C_{C,CO2,t} = C_{D,CO2} + \left(C_{B,CO2} - C_{D,CO2}\right) \cdot e^{\left(-\frac{t}{\theta_D}\right)} \quad (12)$$

Equation 12 described well the experimental data, with a mean R^2 of 0.879 ± 0.156. Overall, θ_D was 53.7 ± 31.3 s, which indicate a fast metabolic change after the switch from light to dark conditions, in accordance with the literature (Masarovičova, 1979). Overall, R_{CO2} was positive, *i.e.* CO_2 emission, in all but two cases, with a range (excluding negative values) of 31–1231 mg m^{-2} h^{-1} and a mean of 359 ± 292 mg m^{-2} h^{-1}. This range is consistent with those previous reports conducted in peatlands from Southern Patagonia, which ranged between 8 and 667 mg m^{-2} h^{-1} using the traditional static chamber method (Pancotto et al., 2021; Barret et al., 2022). Repeatability, R_{CO2} was also evaluated with measurements at 16 locations divided in four transects of 3 m, on three occasions, *i.e.* 2 and 12 days after the first measurement (Table S1). During these measurements, we observed that the temporal variation (same location at different days) was characterized by a mean CV of 33 ± 17% while the mean CV of spatial variation (different locations on the same day) was 58 ± 5%. These values suggest two important patterns. First, that R_{CO2} is relatively well distributed, as compared to $F_{CH4,2}$. Second, that the temporal variation of R_{CO2} is lower than its spatial variation; this pattern resembles the findings for $F_{CH4,2}$.

The CV of the absolute R_{CO2}, noted $|R_{CO2}|$ (Fig. 4A), was within the same range than the CV of $F_{CH4,2}$. In this case the LOD of $|R_{CO2}|$ was estimated to 173 mg m^{-2} h^{-1} and 76% of our measurements were above that limit. As previously done with $F_{CH4,2}$, we also determined how the variation in each measurement propagates to the mean respiration of the complete dataset (Figure 4B). Although with a larger impact than in the case of $F_{CH4,2}$, similar results were obtained. These results suggest that the skirt-chamber allowed the accurate determination of the ecosystem respiration.

3.6. Strengths and perspectives of the skirt-chamber

The skirt-chamber concept, tested for the first time in this work, allowed for the determination of CH_4 emissions and respiration rates in a peatland. For both parameters, the majority of the measurements were above the detection limit of the method and were characterized by a CV within acceptable limits (*i.e.* <33%). By repeating measurements over a 12-days period, similar results were obtained, indicating that these parameters were more homogeneously distributed over time than over space. From the experience acquired during field deployment, the best strategy would be to measure CH_4 emissions and ecosystem respiration according to a three–steps protocol: (i) measurement of ground-air concentration for 5 min, followed by (ii) the installation of the chamber and the immediate pulse injection, waiting 5-7 minutes before (iii) covering the

https://doi.org/10.5194/bg-2023-37
Preprint. Discussion started: 20 February 2023
© Author(s) 2023. CC BY 4.0 License.


chamber with a dark screen for an additional 5 min. Thus, in 15-17 min, CH_4 emission and ecosystem respiration of a specific location can be determined, which suggest that about 20–30 locations could be measured in a reasonable workday (even in remote areas). The main strength of the method is that these parameters can be determined in a minimally intrusive manner and without delay. Moreover, the relatively small size of the skirt-chamber also allows to determine CH_4 emission and respiration with a good spatial resolution, on almost any terrain and vegetation cover. A higher spatial resolution than standard methods would results in a higher probability to detect hotspots, which can represent a very significant fraction of the total emissions. The skirt-chamber seems compatible with the current technological development of lighter, smaller and more energy efficient gas detectors, gaining portability and allowing that a single operator could explore larger peatland extensions.

Compared to standard chambers, we see that the main advantage of the skirt-chamber is, in addition to minimal disturbance and improved spatial resolution, the superior portability for field work in remote locations. Contrastingly, standard chambers, and in particular automatic chambers, offer an incomparable temporal resolution, with minimal field workload. Thus, we conclude that the skirt-chamber concept is a new alternative tool, with specific advantages, that could be advantageously combined with the existing methods, to improve our understanding of greenhouse gas emissions and of the factors controlling them in peatlands.

Supporting Information

One supporting information file (Word Document .docx) containing one Figure and one Table.

Author Contributions

The manuscript was written through contributions of all authors. All authors have given approval to the final version of the manuscript.

Acknowledgements

This project was financially supported by the Cape Horn International Center project (ANID, CHIC-FB210018). ANID, Fondecyt Postdoc (3220809), and Millennium Science Initiative Program (ICN2021_002). Special thanks to Rachele Ossola for her help in preparing the graphical abstract.

https://doi.org/10.5194/bg-2023-37
Preprint. Discussion started: 20 February 2023
© Author(s) 2023. CC BY 4.0 License.

References

Abdalla, M.; Hastings, A.; Truu, J.; Espenberg, M.; Mander, Ü.; Smith, P. Emissions of Methane from Northern Peatlands: A Review of Management Impacts and Implications for Future Management Options. *Ecol. Evol.* **2016**, *6*(19), 7080–7102. https://doi.org/10.1002/ECE3.2469

AR6 Climate Change 2021: The Physical Science Basis — IPCC. https://www.ipcc.ch/report/sixth-assessment-report-working-group-i/ (accessed 2022-08-07).

Aubinet, M.; Vesala, T.; Papale, D. Eddy Covariance: A Practical Guide to Measurement and Data Analysis. 2012. *Springer Atmospheric Sciences* **2012**, *1*, 0–438. https://doi.org/10.1007/978-94-007-2351-1

Barret, M.; Gandois, L.; Thalasso, F.; Martinez-Cruz, K.; Sepulveda-Jauregui, A.; Lavergne, C.; Teisserenc, R.; Aguilar-Muñoz, P.; Gerardo-Nieto, O.; Etchebehere, C.; Dellagnezze, B.; Bovio-Winkler, P.; Fochesatto, G.; Tananaev, N.; Svenning, M. M.; Seppey, C.; Tveit, A.; Chamy, R.; Astorga-España, M. S.; Mansilla, A. O.; van de Putte, A.; Sweetlove, M.; Murray, A. E. A Combined Microbial and Biogeochemical Dataset from High-Latitude Ecosystems with Respect to Methane Cycle. *Sci. Data* **2022**, 9:674. https://doi.org/10.1038/s41597-022-01759-8.

Bracho, R.; Jose, J. J. S. Energy Fluxes in a Morichal (Swamp Palm Community) at the Orinoco Llanos, Venezuela - Microclimate, Water-Vapor and CO2 Exchange. *Photosynthetica* **1990**, *24*, 468–494.

Christiansen, J. R.; Korhonen, J. F. J.; Juszczak, R.; Giebels, M.; Pihlatie, M. Assessing the Effects of Chamber Placement, Manual Sampling and Headspace Mixing on CH4 Fluxes in a Laboratory Experiment. *Plant Soil* **2011**, *343*(1), 171–185. https://doi.org/10.1007/S11104-010-0701-Y

Cobb, A. R.; Hoyt, A. M.; Gandois, L.; Eri, J.; Dommain, R.; Salim, K. A.; Kai, F. M.; Su'ut, N. S. H.; Harvey, C. F. How Temporal Patterns in Rainfall Determine the Geomorphology and Carbon Fluxes of Tropical Peatlands. *Proc. Natl. Acad. Sci. U. S. A.* **2017**, *114* (26), E5187–E5196. https://doi.org/10.1073/pnas.1701090114

Ding, W.; Cai, Z.; Tsuruta, H. Diel Variation in Methane Emissions from the Stands of Carex Lasiocarpa and Deyeuxia Angustifolia in a Cool Temperate Freshwater Marsh. *Atmos. Environ.* **2004**, *38*(2), 181–188. https://doi.org/10.1016/J.ATMOSENV.2003.09.066

Edwards, N. T.; Sollins, P. Continuous Measurement of Carbon Dioxide Evolution From Partitioned Forest Floor Components. *Ecology* **1973**, *54*(2), 406–412. https://doi.org/10.2307/1934349

Fritz, C.; Pancotto, V. A.; Elzenga, J. T. M.; Visser, E. J. W.; Grootjans, A. P.; Pol, A.; Iturraspe, R.; Roelofs, J. G. M.; Smolders, A. J. P. Zero Methane Emission Bogs: Extreme Rhizosphere Oxygenation by Cushion Plants in Patagonia. *New Phytol.* **2011**, *190*(2), 398–408. https://doi.org/10.1111/J.1469-8137.2010.03604.X

Frolking, S.; Talbot, J.; Jones, M. C.; Treat, C. C.; Kauffman, J. B.; Tuittila, E. S.; Roulet, N. Peatlands in the Earth's 21st Century Climate System. *Environmental Reviews* **2011**, *19*, 371–396. https://doi.org/10.1139/A11-014

Griscom, B. W.; Adams, J.; Ellis, P. W.; Houghton, R. A.; Lomax, G.; Miteva, D. A.; Schlesinger, W. H.; Shoch, D.; Siikamäki, J. v.; Smith, P.; Woodbury, P.; Zganjar, C.; Blackman, A.; Campari, J.; Conant, R. T.; Delgado, C.; Elias, P.;

© Author(s) 2023. CC BY 4.0 License.

Gopalakrishna, T.; Hamsik, M. R.; Herrero, M.; Kiesecker, J.; Landis, E.; Laestadius, L.; Leavitt, S. M.; Minnemeyer, S.; Polasky, S.; Potapov, P.; Putz, F. E.; Sanderman, J.; Silvius, M.; Wollenberg, E.; Fargione, J. Natural Climate Solutions. *Proc. Natl. Acad. Sci. U. S. A.* **2017**, *114* (44), 11645–11650. https://doi.org/10.1073/pnas.1710465114

Günther, A. B.; Huth, V.; Jurasinski, G.; Glatzel, S. Scale-Dependent Temporal Variation in Determining the Methane Balance of a Temperate Fen. *Greenhouse Gas Measurement and Management* **2014**, *4*(1), 41–48. https://doi.org/10.1080/20430779.2013.850395

Günther, A.; Barthelmes, A.; Huth, V.; Joosten, H.; Jurasinski, G.; Koebsch, F.; Couwenberg, J. Prompt Rewetting of Drained Peatlands Reduces Climate Warming despite Methane Emissions. *Nat. Commun.* **2020**, *11*(1), 1–5. https://doi.org/10.1038/s41467-020-15499-z

Heusser, C. J. Late Quaternary Vegetation and Climate of Southern Tierra del Fuego. Late Quaternary vegetation and climate of southern Tierra del Fuego. *Quaternary Research* **1989,** 31(3), 396-406. https://doi.org/10.1016/0033-5894(89)90047-1

Hoyos-Santillan, J.; Lomax, B. H.; Large, D.; Turner, B. L.; Lopez, O. R.; Boom, A.; Sepulveda-Jauregui, A.; Sjögersten, S. Evaluation of Vegetation Communities, Water Table, and Peat Composition as Drivers of Greenhouse Gas Emissions in Lowland Tropical Peatlands. *Sci. Total Environ.* **2019**, *688*, 1193–1204. https://doi.org/10.1016/J.SCITOTENV.2019.06.366

Järveoja, J.; Nilsson, M. B.; Crill, P. M.; Peichl, M. Bimodal Diel Pattern in Peatland Ecosystem Respiration Rebuts Uniform Temperature Response. *Nat. Commun.* **2020**, *11*(1), 1–9. https://doi.org/10.1038/s41467-020-18027-1

Juszczak, R. Biases in Methane Chamber Measurements in Peatlands. *Int. Agrophys.* **2013**, *27*(2), 159–168. https://doi.org/10.2478/V10247-012-0081-Z

Kutzbach, L.; Schneider, J.; Sachs, T.; Giebels, M.; Nykänen, H.; Shurpali, N. J.; Martikainen, P. J.; Alm, J.; Wilmking, M. CO2 Flux Determination by Closed-Chamber Methods Can Be Seriously Biased by Inappropriate Application of Linear Regression. *Biogeosciences* **2007**, *4*(6), 1005–1025. https://doi.org/10.5194/BG-4-1005-2007

Lai, D. Y. F.; Roulet, N. T.; Humphreys, E. R.; Moore, T. R.; Dalva, M. The Effect of Atmospheric Turbulence and Chamber Deployment Period on Autochamber CO2 and CH4 Flux Measurements in an Ombrotrophic Peatland. *Biogeosciences* **2012**, *9*(8), 3305–3322. https://doi.org/10.5194/BG-9-3305-2012

Lawson, I. T.; Kelly, T. J.; Aplin, P.; Boom, A.; Dargie, G.; Draper, F. C. H.; Hassan, P. N. Z. B. P.; Hoyos-Santillan, J.; Kaduk, J.; Large, D.; Murphy, W.; Page, S. E.; Roucoux, K. H.; Sjögersten, S.; Tansey, K.; Waldram, M.; Wedeux, B. M. M.; Wheeler, J. Improving Estimates of Tropical Peatland Area, Carbon Storage, and Greenhouse Gas Fluxes. *Wetl. Ecol. Manag.* **2014**, *23*(3), 327–346. https://doi.org/10.1007/S11273-014-9402-2

Lehmann, J. R. K.; Münchberger, W.; Knoth, C.; Blodau, C.; Nieberding, F.; Prinz, T.; Pancotto, V. A.; Kleinebecker, T. High-Resolution Classification of South Patagonian Peat Bog Microforms Reveals Potential Gaps in Up-Scaled CH4 Fluxes by Use of Unmanned Aerial System (UAS) and CIR Imagery. *Remote Sens.* **2016**, *8*, 173. https://doi.org/10.3390/RS8030173

© Author(s) 2023. CC BY 4.0 License.

Leifeld, J.; Menichetti, L. The Underappreciated Potential of Peatlands in Global Climate Change Mitigation Strategies. *Nature Communications* **2018**, *9*, 1–7. https://doi.org/10.1038/s41467-018-03406-6

Levenspiel, O. Chemical Reaction Engineering, 3rd ed.; Anderson, W., Hepburn, K., Santor, K., Eds.; Times Roman by Bi-Comp Inc, **1999**; pp 4140–4143.

Limpert, K. E.; Carnell, P. E.; Trevathan-Tackett, S. M.; Macreadie, P. I. Reducing Emissions From Degraded Floodplain Wetlands. *Front. Environ. Sci.* **2020**, *8*, 8. https://doi.org/10.3389/FENVS.2020.00008/BIBTEX

Livingston, G.; Hutchinson, J. Enclosure-Based Measurement of Trace Gas Exchange: Applications and Sources of Error. In Biogenic trace gases: measuring emissions from soil and water; Matson, P., Harris, R., Eds.; R.C.: Oxford, UK, **1995**; pp 14–51.

Masarovičova, E. Relationships between the CO2 Compensation Concentration, the Slope of CO2 Curves of Net Photosynthetic Rate and the Energy of Irradiance. *Biol. Plantarum* **1979**, *21*(6), 21 (6), 434–439. https://doi.org/10.1007/BF02889485

Münchberger, W.; Knorr, K. H.; Blodau, C.; Pancotto, V. A.; Kleinebecker, T. Zero to Moderate Methane Emissions in a Densely Rooted, Pristine Patagonian Bog - Biogeochemical Controls as Revealed from Isotopic Evidence. *Biogeosciences* **2019**, *16*(2), 541–559. https://doi.org/10.5194/BG-16-541-2019

Page, S.; Mishra, S.; Agus, F.; Anshari, G.; Dargie, G.; Evers, S.; Jauhiainen, J.; Jaya, A.; Jovani-Sancho, A. J.; Laurén, A.; Sjögersten, S.; Suspense, I. A.; Wijedasa, L. S.; Evans, C. D. Anthropogenic Impacts on Lowland Tropical Peatland Biogeochemistry. *Nat. Rev. Eart. Environm.* **2022**, 3 (7), 426–443. https://doi.org/10.1038/s43017-022-00289-6

Pancotto, V.; Holl, D.; Escobar, J.; Castagnani, M. F.; Kutzbach, L. Cushion Bog Plant Community Responses to Passive Warming in Southern Patagonia. *Biogeosciences* **2021**, *18*(16), 4817–4839. https://doi.org/10.5194/BG-18-4817-2021

Pavelka, M.; Acosta, M.; Kiese, R.; Altimir, N.; Brümmer, C.; Crill, P.; Darenova, E.; Fu□.; Gielen, B.; Graf, A.; Klemedtsson, L.; Lohila, A.; Longdoz, B.; Lindroth, A.; Nilsson, M.; Maranón Jiménez, S.; Merbold, L.; Montagnani, L.; Peichl, M.; Pumpanen, J.; Serrano Ortiz, P.; Silvennoinen, H.; Skiba, U.; Vestin, P.; Weslien, P.; Janous, D.; Kutsch, W. Standardisation of chamber technique for CO2, N2O and CH4 fluxes measurements from terrestrial ecosystems. *Int. Agrophys* **2018**, 32, 569–587. https://doi.org/10.1515/intag-2017-0045

Pirk, N.; Mastepanov, M. Calculations of Automatic Chamber Flux Measurements of Methane and Carbon Dioxide Using Short Time Series of Concentrations. *Biogeosciences* **2015**, 14593–14617. https://doi.org/10.5194/bgd-12-14593-2015

Ribeiro, K.; Pacheco, F. S.; Ferreira, J. W.; de Sousa-Neto, E. R.; Hastie, A.; Krieger Filho, G. C.; Alvalá, P. C.; Forti, M. C.; Ometto, J. P. Tropical Peatlands and Their Contribution to the Global Carbon Cycle and Climate Change. *Glob. Chang. Biol.* **2021**, *27*(3), 489–505. https://doi.org/10.1111/GCB.15408

Rozzi, R.; Armesto, J. J.; Gutiérrez, J.; Massardo, F.; Likens, G.; Anderson, C. B.; Poole, A.; Moses, K.; Hargrove, G.; Mansilla, A.; Kennedy, J.H.; Willson, M.; Jax, K.; Jones, C.; Callicott, J. B.; Kalin. M. T. Integrating ecology and environmental ethics: Earth stewardship in the southern end of the Americas. *BioScience* **2012**, 62(3), 226-236. https://doi.org/10.1525/bio.2012.62.3.4

https://doi.org/10.5194/bg-2023-37
Preprint. Discussion started: 20 February 2023
© Author(s) 2023. CC BY 4.0 License.

Rozzi, R.; Massardo, F.; Anderson, C.; Heidinger, K.; J. Silander Jr. Ten Principles for biocultural conservation at the southern tip of the Americas: The approach of the Omora Ethnobotanical Park. *Ecology and Society* **2006**, 11(1), 43. http://www.ecologyandsociety.org/vol11/iss1/art43/

Swails, E.; Hergoualc'h, K.; Verchot, L.; Novita, N.; Lawrence, D. Spatio-Temporal Variability of Peat CH4 and N2O Fluxes and Their Contribution to Peat GHG Budgets in Indonesian Forests and Oil Palm Plantations. *Front. Environ. Sci.* **2021**, *9*, 48. https://doi.org/10.3389/FENVS.2021.617828/BIBTEX

United Nations Environment Programme (UNEP). Resolution 4/16. Conservation and Sustainable Management of Peatlands - Resolution Adopted by the United Nations Environment Assembly on 15 March **2019**. https://wedocs.unep.org/20.500.11822/30675

Wright, E. L.; Black, C. R.; Turner, B. L.; Sjögersten, S. Environmental Controls of Temporal and Spatial Variability in CO2 and CH4 Fluxes in a Neotropical Peatland. *Glob. Chang. Biol.* **2013**, *19*(12), 3775–3789. https://doi.org/10.1111/GCB.12330

Yu, Z.; Beilman, D. W.; Frolking, S.; MacDonald, G. M.; Roulet, N. T.; Camill, P.; Charman, D. J. Peatlands and Their Role in the Global Carbon Cycle. *Eos* **2011**, *92* (12), 97–98. https://doi.org/10.1029/2011EO120001